



Chemically robust superhydrophobic surfaces with a self-replenishing nanoscale liquid coating

Xiaoteng Zhou¹ | Pranav Sudersan¹  | Diego Diaz¹ | Benjamin Leibauer¹ | Chirag Hinduja¹ | Fahimeh Darvish¹ | Pravash Bista¹ | Lukas Hauer¹ | Manfred Wagner¹ | Werner Steffen¹ | Jie Liu^{1,2,3} | Michael Kappl¹ | Hans-Jürgen Butt¹ 

¹Max Planck Institute for Polymer Research, Mainz, Germany

²Key Laboratory of Green Printing, Institute of Chemistry, Chinese Academy of Sciences, Beijing, China

³School of Chemical Sciences, University of Chinese Academy of Sciences, Beijing, China

Correspondence

Jie Liu, Michael Kappl, and Hans-Jürgen Butt, Max Planck Institute for Polymer Research, Ackermannweg 10, 55128 Mainz, Germany. Email: liujie123@iccas.ac.cn, kappl@mpip-mainz.mpg.de and butt@mpip-mainz.mpg.de

Funding information

European Research Council (ERC) under the European Union's Horizon 2020 research and innovation program, Grant/Award Numbers: 883631, DYNAMO; German Research Society via the CRC 1194, Grant/Award Numbers: 265191195, C07N

Abstract

Due to poor chemical robustness, superhydrophobic surfaces become susceptible to failure, especially in a highly oxidative environment. To ensure the long-term efficacy of these surfaces, a more stable and environmentally friendly coating is required to replace the conventional salinization layers. Here, soot-templated surfaces with re-entrant nanostructures are precoated with polydimethylsiloxane (PDMS) brushes. An additional nanometer-thick lubricant layer of PDMS was then applied to increase chemical stability. The surface is superhydrophobic with a nanoscale liquid coating. Since the lubricant layer is thin, ridge formation is suppressed, which leads to low drop sliding friction and fast drop shedding. By introducing a bottom "reservoir" of a free lubricant as an oil source for self-replenishing to the upper layer, the superhydrophobic surface becomes more stable and heals spontaneously in response to alkali erosion and O₂ plasma exposure. This design also leads to a higher icing delay time and faster removal of impacting cooled water drops than for uncoated surfaces, preventing icing at low temperatures.

INTRODUCTION

Superhydrophobic surfaces have been proposed as promising materials for a variety of applications, including heat transfer,^{1,2} self-cleaning,³ fuel filters,⁴ water harvesting,⁵ anti-icing,^{6,7} and so forth. These surfaces mainly rely on hierarchical micro/nanostructures^{8–10} and low-surface-tension chemistry.^{11,12} A general challenge for these surfaces is the easily damaged surface structure and chemistry under physical contact or oxidation.¹³ Most recent studies mainly focus on preventing physical damages¹³; for example, a sacrificing coating layer¹⁴ and an "armor" surface frame³ are

designed. Rarely have strategies been reported to prevent the formation of chemical defects^{15,16} by reactant oxidization¹⁷ of the low-surface-tension silane coatings on these rough structures.^{18–20}

Generally, artificial superhydrophobic surfaces need to be modified with organosilanes,¹¹ such as fluorinated long-chain alkyl silanes²¹ or methylated medium-chain alkyl silanes,²² to lower the surface energy. These silanes limit the chemical stability of the surfaces because of a hydrolysis reaction between the Si–O bond in the silane and the OH[−] in the solution.¹⁷ Moreover, atoms present in the side chain of the silanes can also be oxidized when exposed to plasma discharging.²³ This limits the use of these surfaces in

This is an open access article under the terms of the [Creative Commons Attribution](https://creativecommons.org/licenses/by/4.0/) License, which permits use, distribution and reproduction in any medium, provided the original work is properly cited.

© 2024 The Authors. *Droplet* published by Jilin University and John Wiley & Sons Australia, Ltd.

spacecraft launch, water treatment, semiconductor manufacturing, and energy generation in which strong oxidizing environments exist. With respect to a low-temperature environment, the hydrophobic segment in the organosilane combined with the nanoroughness will provide more nucleation sites for the cooled water.^{24,25} This will result in a high nucleation rate and a low delay icing time, which will result in the impact drop being pinned on the cooled superhydrophobic surface.^{26,27} In addition, the widely used fluorinated silanes pose a threat to the environment and bioaccumulate in humans, animals, and plants. Therefore, fluorine-free alternatives are urgently needed.²⁸

By combining superhydrophobicity and so-called liquid-infused surfaces (LISs), we intend to make a step forward to overcome these limits. A LIS is a rough or porous surface that is infused with oil,²⁹ providing protection against corrosion³⁰ and enabling self-healing³¹ or self-replenishing.³² However, in contrast to superhydrophobic surfaces, they still show high normal adhesion, which requires significant effort to remove droplets and results in low drop velocity. Additionally, the depletion of the oil layer limits their functionality to a finite time or number of drops. Given the advantages of the liquid layer in stabilizing surface chemical properties, it is promising to apply a liquid layer as a coating for superhydrophobic surfaces. While some previous work has attempted to combine a liquid layer with micro-scale structures to create a lubricant-air interface,^{33–36} the resulting oil layer tends to have significant thickness (>1 μm). Consequently, an oil wedge is formed at the three-phase contact line, leading to a decreased drop shedding velocity. It is still a challenge to fabricate a superhydrophobic surface with high drop shedding velocities while also being chemically stable, self-replenishing, and icephobic.³⁷

Here, we propose a general strategy for creating chemically robust superhydrophobic surfaces by replacing the conventional solid coating with a replenishable liquid film. To combine the advantage of a liquid coating but prevent the formation of large oil menisci, a nanoscale liquid coating is successfully fabricated. By incorporating a precoated layer, a low-surface-tension liquid polydimethylsiloxane (PDMS) film can be subsequently stabilized with the help of the chemically identical interaction and the high roughness of the surface. The surface shows a high drop shedding velocity similar to that on a nonoil-coated superhydrophobic surface. Benefiting from the protection and replenishment of the flowable liquid coating, the superhydrophobic surface demonstrates outstanding stability, resisting alkaline corrosion and oxygen aging. Such a design, which combines superhydrophobicity and lubrication in one surface, significantly reduces lubricant depletion from the surface. The liquid coating, resulting in a smooth liquid-air interface, delays ice nucleation and accelerates liquid removal before freezing, enhancing the surface's performance at low temperature.

RESULTS AND DISCUSSION

The SiO_2 candle-soot-templated surface⁹ was prepared as a model surface with a nanoscopic re-entrant structure (Figure 1a). It is easy to prepare without the need for complex equipment. A large area of

similar coating can also be obtained by liquid flame spray using a well-designed setup.³⁸ The soot layer was typically $H_0 = 40 \mu\text{m}$ thick (Supporting Information: Figure S1). Liquid PDMS preferentially wets a smooth PDMS brush-modified surface,^{39,40} rather than fluorinated surfaces; on a smooth surface, PDMS forms a static contact angle of 6° rather than $\approx 50^\circ$ (Supporting Information: Figure S2). Thus, the soot-templated surface was modified with PDMS chains first.⁴¹ We call it a "PDMS brush," although the chains may be attached at random points of the chain and there may be multiple links. The nature of the bond is not clear. We assume that it is covalent because the PDMS chains cannot be removed by exposing them to a good solvent (Supporting Information: Section 1). We use the abbreviation PDMS-SH (PDMS brush-modified superhydrophobic) surface to refer to this surface. Since PDMS has a glass transition temperature of around -125°C , the brush is in an almost liquid-like state.⁴² Low concentrations of PDMS (viscosity: 100 cst; molar mass M_w : 6000 g/mol) dissolved in toluene were spin-coated onto PDMS-SH surfaces (4000 rpm, 60 s). The liquid PDMS was chemically identical^{40,43} to the PDMS brush because of the same molecular weight and chemical structure. After solvent evaporation, due to mixing entropy, oil diffuses into the grafted PDMS and swells the brush (Figure 1a). This kind of surface has a similar mechanical stability as that reported for a superhydrophobic soot-templated surface (Supporting Information: Figure S4).⁹

After the preparation, we could observe a liquid nanofilm surrounding the nanostructures from the force measurement by atomic force microscopy (AFM) (Figure 1b,c). AFM is an effective tool to detect the presence of oil on the nanoscale features because it can locally probe capillary forces even on a rough surface⁴⁴ (Supporting Information: Section 2). The "jump-in distance" illustrates the thickness T of the fluid layer (Figure 1b). When the AFM tip approached a PDMS-SH surface, the tip jumped from an average distance of about 10 nm (Figure 1b, blue symbols). This value is the same order of magnitude as the brush thickness. Similar jump-in distances were observed on smooth PDMS-coated surfaces as reported before.⁴³ On the liquid-coated PDMS brush-modified superhydrophobic (L-PDMS-SH) (7.5%) surface, approaching force curves showed a long jump-in distance (Figure 1b, red symbols) before hard contact was established. The average thickness of the nanoscale oil layer was around 20 nm, and it has a wide range from 10 to 100 nm. These large jump-in distances demonstrate that the liquid swells the brush roughly by a factor of 2–3.

We used the quantitative imaging (QI) mode of the AFM, where a force-distance curve is obtained in each pixel of an image and the jump-in distance is extracted using a custom Python analysis script. From the resulting map (Figure 1c), we can see the oil distribution visually. For the PDMS-SH surface, the jump-in distance is lower than 10 nm over the whole surface, which illustrates a solid coating. For the L-PDMS-SH (7.5%) surface, we can see that the re-entrant structures are covered with a thin liquid layer. For a liquid-infused fluorinated superhydrophobic (L-F-SH, 7.5%) surface, the oil infused into the structure, but we could not detect continuous free PDMS on top (Supporting Information: Figure S7). We conclude that the oil can

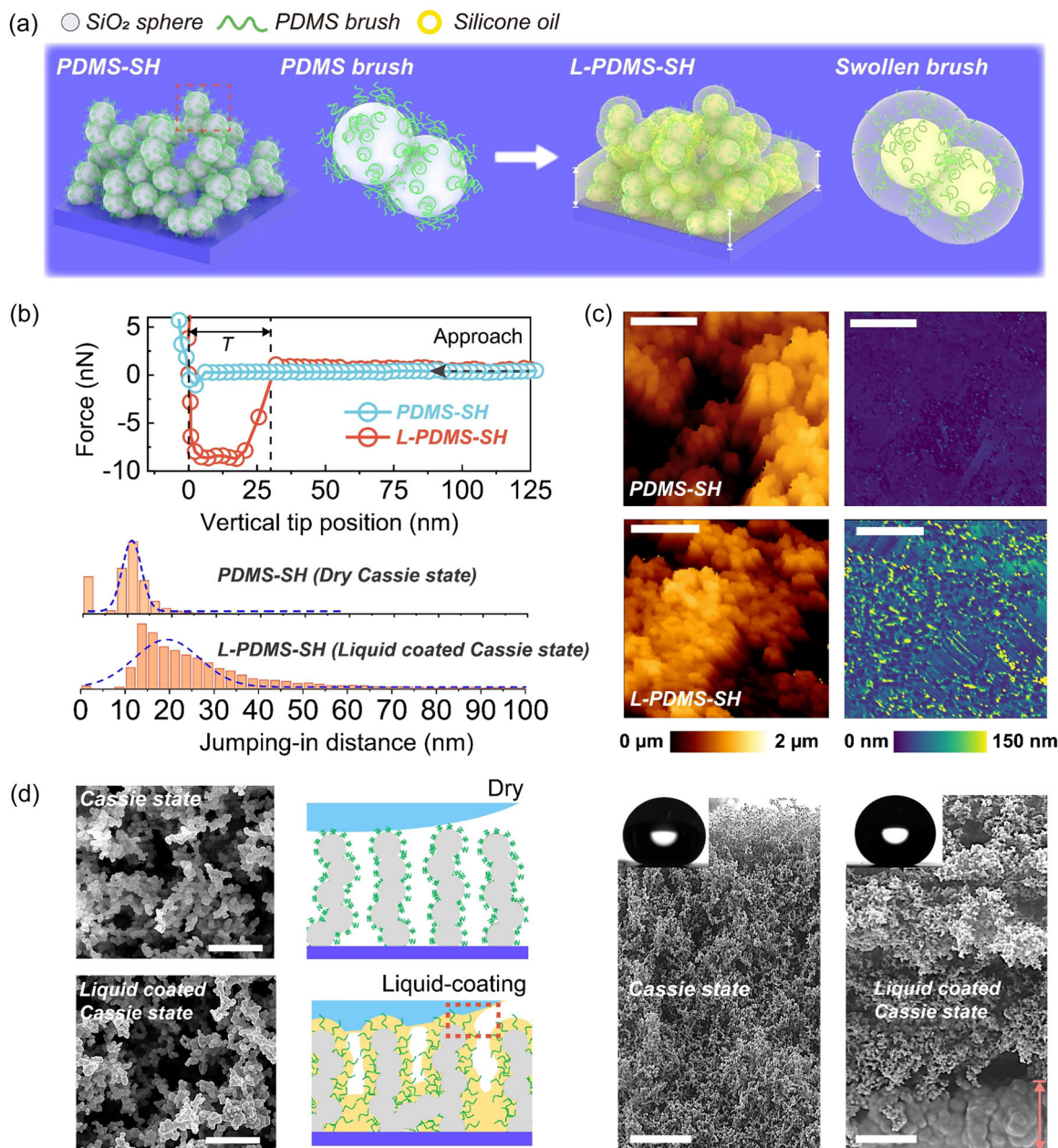


FIGURE 1 Liquid-coated polydimethylsiloxane brush-modified superhydrophobic (L-PDMS-SH) surface. (a) Schematic of the preparation and structures of PDMS brush-modified superhydrophobic (PDMS-SH) and the L-PDMS-SH surface. (b) Approaching force curve measured on PDMS-SH, L-PDMS-SH (7.5%) surfaces and histogram of the frequency count of jump-in distances on these surfaces. (c) Atomic force microscopy topography (left) of PDMS-SH, L-PDMS-SH (7.5%) surfaces, and the corresponding maps (right) of the distribution of liquid coating thickness. Scale bar: 500 nm. (d) Scanning electron microscopy images of a dry and a liquid-coated Cassie state. Scale bar top view (left): 10 μm ; cross-section view (right): 5 μm . The middle scheme illustrates the nanoscale liquid coating structure. The red dotted frame illustrates the neglectable nanoscale deformation near the contact line. The red arrow in the cross-section view indicates the thickness of the bottom oil reservoir.

only spontaneously cover the PDMS-coated surfaces because they are chemically identical but not the fluorinated ones.

Our oil layer in the PDMS brush is much thinner than previously reported liquid-coated surfaces.^{34,45,46} Since its thickness is only nanometers, it cannot be discerned in scanning electron microscopy (SEM) images (Figures 1d and 2). The morphology of the upper structure closely resembles that of the dry superhydrophobic surface.

A $\approx 5\text{-}\mu\text{m}$ -thick oil layer (bottom liquid “reservoir”) is visible only at the lower portion of the surface in the cross-sectional view (Figure 1d). By assimilating the findings from AFM force curves, it can be inferred that a nanoscale oil layer envelops the nanosphere structures of the soot-templated surface.

The lubricating PDMS also forms a bottom oil layer as a “pool” underneath the nanostructures (Figure 2a). It can be used like a

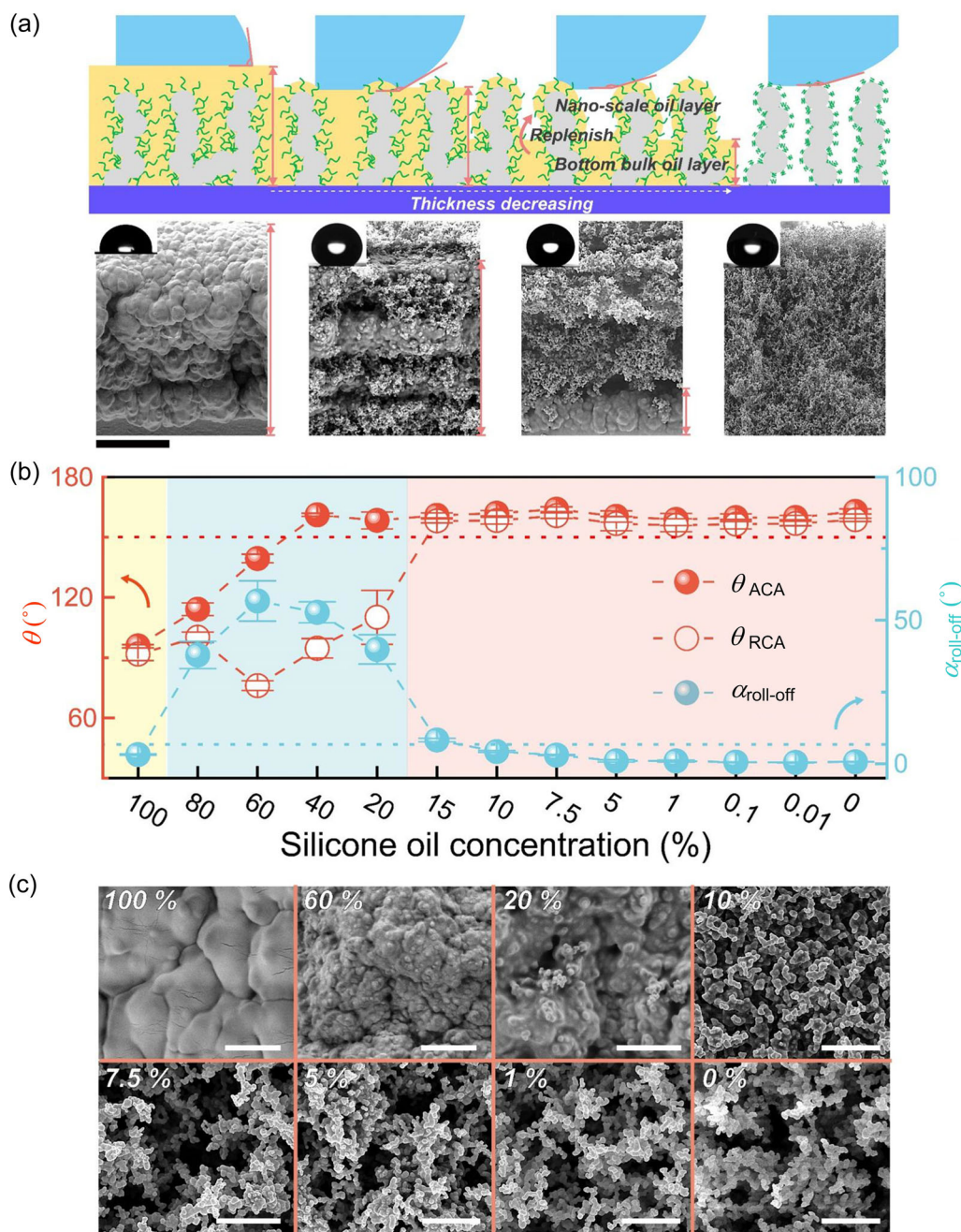


FIGURE 2 Wetting property transition. (a) Illustration of the oil structure in liquid-coated polydimethylsiloxane brush-modified superhydrophobic (L-PDMS-SH) surfaces resulting from the different concentrations of oil infused (from left to right: 100%, 20%, 7.5%, and 0%). Scanning electron microscopy (SEM) images show the cross-section morphologies of the surface with different bottom oil layer thicknesses; scale bar: 10 μ m. Inset images show the static contact angles of water drops on the corresponding morphology. (b) Advancing and receding contact angles (θ_{ACA} and θ_{RCA}) and roll-off angles ($\alpha_{roll-off}$) of 10 μ L of water on the L-PDMS-SH surfaces on infusing different concentrations of silicone oil. Red part (■): Superhydrophobic state. Blue part (■): Slippery Wenzel state. Yellow part (■): Slippery state. (c) SEM images of the top views of the L-PDMS-SH surfaces after infusing different concentrations of liquid polydimethylsiloxane (PDMS). Scale bar: 0%–7.5%, 1 μ m; 10% and 20%, 2 μ m; 60% and 100%, 10 μ m.

“gland” in animals for self-replenishing of the nanofilm on top when it is depleted. In this way, liquid-coated self-replenishing surfaces, denoted by L-PDMS-SH, are generated. We can adjust the thickness of the bottom oil layer by choosing different concentrations of PDMS-in-toluene solutions in spin-coating. On spin-coating 100% silicone oil, the whole soot-templated layer was full of liquid, which

can be considered as a LIS. On using the PDMS solutions, the thickness of the bottom oil layer decreased below the maximum height of the nanoscopic SiO₂ structures. During spin-coating, the whole soot-templated SiO₂ structure is filled with solution. After toluene evaporation, only silicone oil will be left which results in a thinner bottom bulk oil layer than that when coating the surface with

pure oil. The wetting properties of L-PDMS-SH surfaces depend on the thickness of the bottom oil (Figure 2a,b) and the static contact angle is in agreement with the previous theoretical results (Supporting Information: Section 3). When the oil concentration was below 15%, the surface was superhydrophobic. The infusing oil viscosity did not affect the apparent advancing and receding contact angles, because the liquid layer is thin and their chemistry is almost similar (Supporting Information: Figure S7).³⁵

When the oil concentration ranged from 20% to 60%, no Cassie state was formed (Figure 2b) and it can be considered as a slippery Wenzel state as reported before.⁴⁶ When the surface was infused with pure oil, a slippery surface with a smooth oil-air interface was formed.

To visualize the interface of the L-PDMS-SH surfaces, which is related to the wetting property,⁴⁷ we infused the PDMS-SH surfaces with a mixture of vinyl-terminated PDMS ($M_w = 6000\text{--}8000\text{ g/mol}$, 100 cst; Gelest) and polymethylhydrosiloxane (Sigma-Aldrich) at a ratio of 9:1. Five microliters of 0.05 wt% and Pt catalyst (platinum-1,3-divinyl-1,1,3,3-tetramethyldisiloxane; Gelest) dissolved in toluene were added. The mixture was diluted into 60, 20, 10, 7.5, 5, and 1 wt% in toluene. The solutions were spin-coated immediately on the PDMS-SH surface and annealed at 80°C for 2 h to cross-link the mixture. Then, SEM images were taken in vacuum (Figure 2c). When the surface was infused with pure oil (100%), it was hard to see the re-entrant structure. Air gaps in the soot-templated structure start to appear after the oil concentration decreased to 20%. When the oil concentration decreased to 10%, some thick oil still remains outside the porous structure. For this reason, we use L-PDMS-SH surfaces with a solution concentration below 10% in the following tests. Once the infusing oil concentration was below 10%, the topography of the L-PDMS-SH surface was the same as that of the nonoil-infused surface.

To further characterize difference in the wetting property, we carried out drop impact and drop sliding experiments. Four microliters of Milli-Q water drops were ejected from a needle controlled by a syringe pump at a height of 2 cm. The dimensionless Weber number We is 10.9 ($We = \rho U_0^2 D / \gamma$, where ρ is the density, U_0 is the impacting velocity, D is the diameter of the drop, and γ is the liquid-air surface tension). Drop impact was recorded using a Photron Fastcam Mini UX100 high-speed camera (5000 fps) with a $\times 2$ lens. Impact water drops can rebound from superhydrophobic PDMS-SH and L-PDMS-SH (7.5%) surfaces. However, the drop impact dynamics differed (Figure 3a and Supporting Information: Section 4). On PDMS-SH, the contact time $\tau = 10\text{ ms}$, while on the L-PDMS-SH (7.5%) surface, we observed a contact time $\tau = 18\text{ ms}$ (Figure 3b). The restitution coefficient, $e = U_R / U_0$ (where U_R is the velocity at the moment of rebound), is higher for the PDMS-SH surface (Supporting Information: Figure S10) and drops disperse faster. The contact time of 10 ms for PDMS-SH agrees with the result obtained from the inverse of the first resonance frequency of drops. At the limit of low viscosity, the first resonance frequency is at an oscillation period $\tau = \pi \sqrt{\rho R^3 / 2\gamma} = \sqrt{3\pi\rho V / 8\gamma}$. Here, R is the initial radius of the drop, ρ is the density of the liquid, and V is the drop volume.^{48–50} Inserting $\gamma = 0.072\text{ N/m}$ leads to $\tau = 8\text{ ms}$. On the

L-PDMS-SH surface, oil is transferred to the drop surface, reducing its surface energy. However, even if we take $\gamma = 0.058\text{ N/m}$, the calculated contact time is only $\tau = 9\text{ ms}$. Thus, more energy is dissipated on L-PDMS-SH than on PDMS-SH surfaces during the impact process. We suggest that the spreading of the oil layer on the drop's surface and the resulting Marangoni flow lead to this energy dissipation, resulting in a longer contact time.⁵¹

Water drops slide differently on L-PDMS-SH surfaces in three wetting states (Figure 3c,d). On PDMS-SH and L-PDMS-SH (5%) surfaces, water drops rolled over the surface at a low tilt angle ($< 5^\circ$) with high contact angles. For a 33 μL drop sliding over the L-PDMS-SH (5%) surface (titling angle: 40°) for a distance of 4 cm, the maximum velocity was $\approx 0.8\text{ m/s}$ (Figure 3d). This velocity is comparable to that observed on a dry superhydrophobic surface (Supporting Information: Figure S12). Thus, drop friction on our nanoscopic liquid-infused surfaces is almost similar to dry superhydrophobic surfaces. At 20%, the advancing angle remained high and the receding contact angle decreased to around 90° (Figure 2b), resulting in a high sliding angle (Figure 3c). The maximum velocity after sliding 4 cm was 0.6 m/s, which is lower than that on a PDMS-SH surface. For the fully slippery state achieved by infusing pure PDMS, the sliding process was consistent with previous observations on LIS, showing a low sliding angle but low drop velocity. Furthermore, the increase in drop velocity with drop number (Figure 3d, right) indicates oil depletion typical for LIS. The main factor influencing drop movement and friction is the liquid layer thickness. For a micrometer-thick oil layer, a continuous meniscus wedge is formed, resulting in high dissipation caused by dragging this wedge over the surface (Supporting Information: Figure S13). For the nanoscale liquid layer, the formation of such a liquid wedge is suppressed, which results in less dissipation (Figure 1d). The friction force caused by dragging a liquid wedge across the surface is absent.^{52,53} Lower friction forces lead to a higher sliding velocity. The drop velocity on different surfaces can be theoretically determined by the energy dissipation based on previous models (Supporting Information: Section 4).⁵⁴

For the silane-modified superhydrophobic surface, OH^- or H^+ ions in the contact liquid cause hydrolysis of the Si-O bond (Figure 4a). Using oxygen plasma, atoms in the side chain can be oxidized. In our design, we added a flowable oil layer above the PDMS brush. It can act as a sacrificial layer to protect the swollen brush and improve the surface's chemical stability. This continuous oil layer can also be replenished by the deposited bottom oil, leading to long-term chemical stability.

To analyze the chemical stability of the surfaces, we measured the dynamic contact angles of an aqueous drop with different pH values on F-SH, PDMS-SH, and L-PDMS-SH (7.5%) surfaces first. The drops with different pH values were prepared by diluting 0.1 M H_2SO_4 aqueous (pH = 1) and 0.1 M KOH (pH = 14) to a certain concentration. They all showed receding contact angles above 150° and low roll-off angles (Supporting Information: Figure S14). However, in real applications, the surface needs to be stable for a long time. We conducted experiments in which we applied alkali KOH drops (pH = 14) to the surface and allowed them to slide for different time

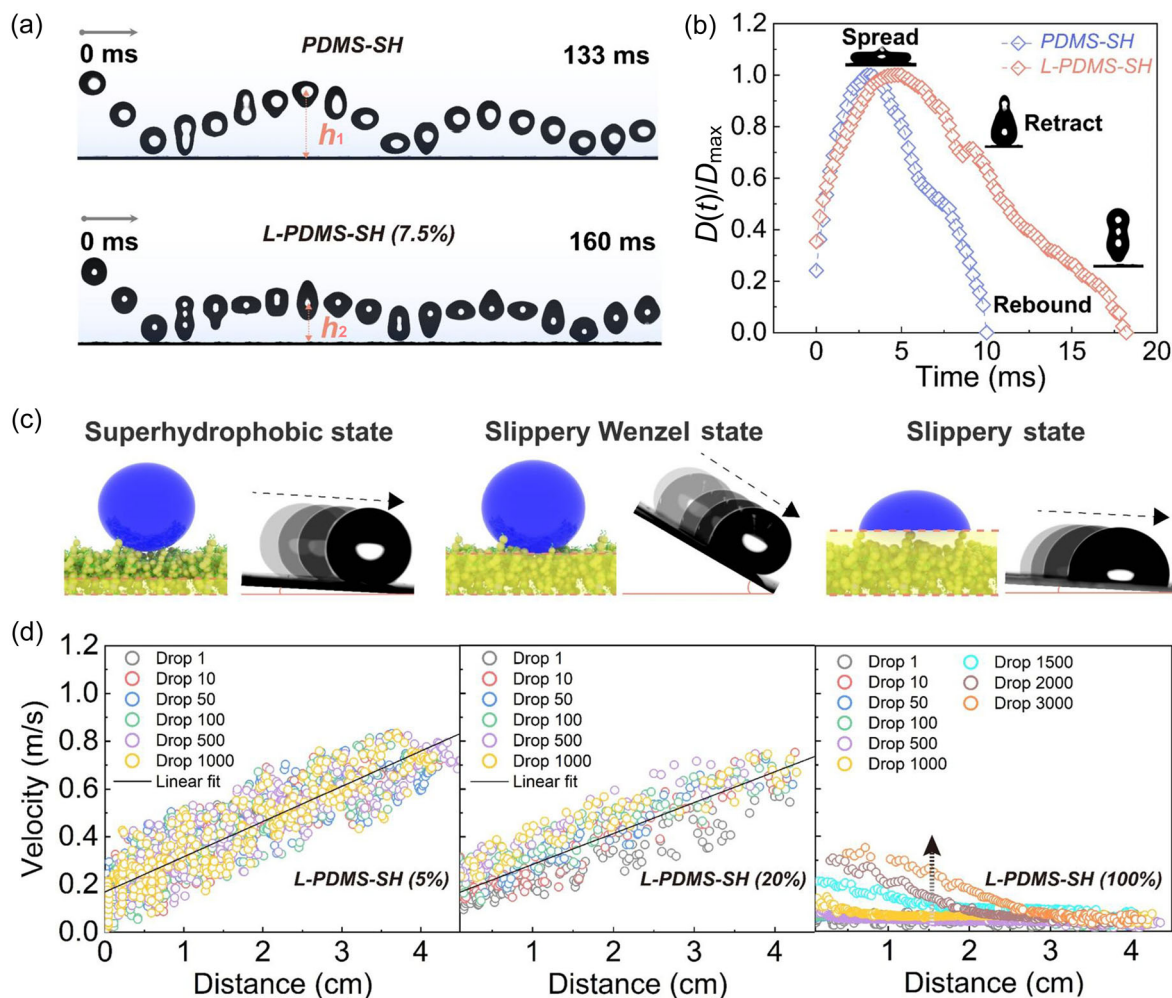


FIGURE 3 Drop dynamics. (a) Four microliters of drop impact on PDMS-SH and liquid-coated PDMS brush-modified superhydrophobic (L-PDMS-SH) (7.5%) surfaces ($We = 10.9$) and (b) time dependence of the scaled contact radius $D(t)/D_{max}$. (c) Three wetting states are indicated by the corresponding schematics and video sequences of 10 μL water drop sliding over L-PDMS-SH surfaces with infusing oil concentrations of 5%, 20%, and 100% (images were recorded at intervals of 0.2 s). (d) Drop velocity versus position on L-PDMS-SH in these three wetting states. The results were measured on a 40° tilted platform with 33 μL water drops. PDMS-SH, polydimethylsiloxane brush-modified superhydrophobic.

periods at a constant velocity (drop size: 45 μL ; Ismatec® Reglo digital miniflex pump; pump speed: 10 $\mu\text{L}/\text{s}$). Then, the contact angle of water was measured in the drop sliding path. F-SH and PDMS-SH surfaces lost their superhydrophobicity after ≈ 100 min (Figure 4b). For L-PDMS-SH (7.5%) surfaces, the surface failed after 800 min treatment, and was thus almost a factor 7 longer. This observation indicates that the oil coating and self-replenishment from the bottom layer prevent the alkali drop from contacting the solid part directly and prolongs the lifetime. This interpretation is supported by the observation that once the L-PDMS-SH fails, AFM experiments no longer showed a liquid layer on the surface (Supporting Information: Figure S15).

The chemical stability of the surface after acid ($\text{pH} = 1$) drop sliding was tested in the same way. Acid degradation for Si-O bonds has been reported to be much lower than that of alkali.¹⁷ Thus, the contact angle hysteresis on F-SH and L-PDMS-SH (7.5%) surfaces was still below 10° after 1000 min (Figure 4c) and the nanoscale oil layer on L-PDMS-SH could be detected after 1000 min of acid treatment (Supporting

Information: Figure S16). In contrast, contact angle hysteresis slightly increases on the PDMS-SH surface after 1000 min. That is because some PDMS chains on top were slowly degraded by the acid. Comparing these results, we know that the enhanced stability is because of the sacrificial nanoscale oil layer. The OH^- ions in the drop will react with the Si-O bond in the liquid part first. Then, because of the high degradation rate of alkali, the nanoscale oil layer will be used out and the replenishment will not be possible. The protected silane can be degraded as the other two surfaces after that, but this process extends the failure time considerably.

Plasma is known to activate the surface and change the interfacial chemical composition.⁵⁵⁻⁵⁷ We compared the wettability of L-PDMS-SH (7.5%), PDMS-SH, and F-SH surfaces after oxygen plasma treatment (power: 20 W; time: 30 s; Diener electronic GmbH). The results show that for F-SH, one cycle of plasma treatment was sufficient to make the surface superhydrophilic. It remained superhydrophilic for at least 24 h (Figure 4d). For L-PDMS-SH (7.5%), the

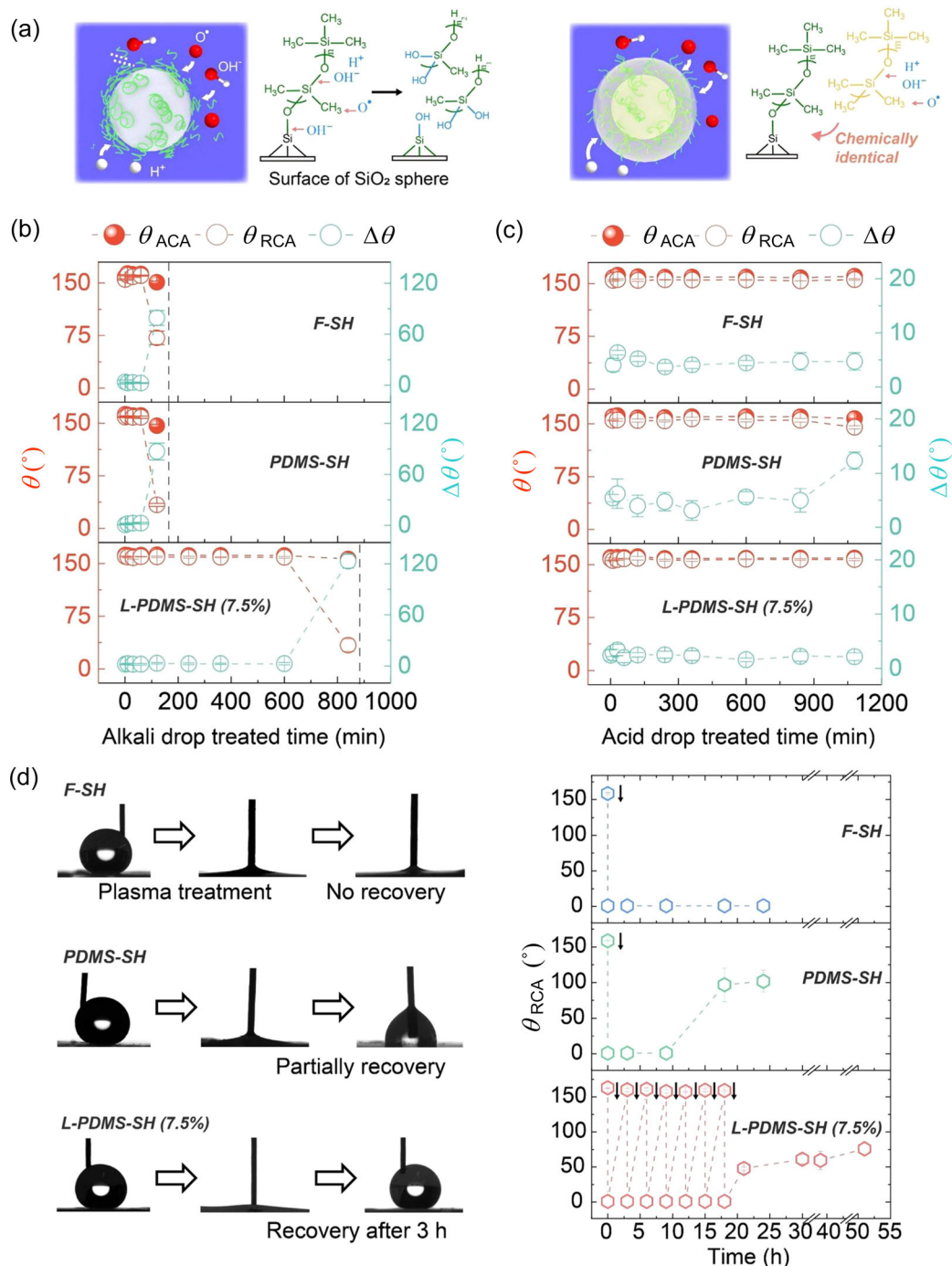


FIGURE 4 Enhanced chemical stability. (a) The diagram shows the possible mechanism of how the liquid coating protects the bonded organosilane from degradation in strong oxidation to enhance chemical stability. (b and c) Changes in advancing and receding contact angles (θ_{ACA} and θ_{RCA}) and hysteresis ($\Delta\theta$) of 10 μ L of water on the surfaces (b) after alkali drops and (c) after acid drops slide off fluorinated superhydrophobic surface (F-SH), polydimethylsiloxane brush-modified superhydrophobic (PDMS-SH), and liquid-coated PDMS brush-modified superhydrophobic (L-PDMS-SH (7.5%)) surfaces for different time periods (tilting angle = 50°, 15 drops/min). (d) Change in the receding contact angle of 10 μ L of water on F-SH, PDMS-SH, and L-PDMS-SH (7.5%) surfaces after O₂ plasma treatment (power: 20 W; time: 30 s). The black arrows inside represent plasma treatment carried out once.

receding contact angle decreased to zero after one plasma treatment. The AFM experiments demonstrated that the nanoscale oil layer still existed after plasma treatment (Supporting Information: Figure S17). However, on placing the surface at room temperature (25–30°C) for 3 h, it recovered. Water drops formed a Cassie state again. We

attribute this recovery to a self-replenishing process of the oil from the bottom. Oil from the bottom layer diffuses upward following the gradient in surface energy created by the plasma. These PDMS chains may also react with the SiO₂ surface, or they may be cross-linked during this process. Experimentally, we observed that after seven

cycles of plasma treatment, the surface no longer recovers to the superhydrophobic state even after 24 h.

We also characterized the wettability change of PDMS-SH after plasma treatment. The surface became superhydrophilic after one cycle of plasma treatment. After being placed at room temperature for 21 h, the water receding contact angle increased to more than 90° within 21 h, but the surface remained in the Wenzel state. Comparing this observation to the result on the L-PDMS-SH (7.5%) surface, we conclude that the recovery to the Cassie state after plasma treatment is caused by the flow and exchange of the bottom oil layer and the top oil nanofilm.

The chemical stability of the superhydrophobic L-PDMS-SH surface relies on the existence of the liquid coating and the replenishment by free PDMS from the bottom. For this reason, we further analyze the oil depletion. For the drop dynamics characterization, we can easily see the lubricate depletion by that if there is an obvious velocity change with the drop number increasing when the lubrication layer is thick. However, for the designed liquid-coated superhydrophobic surface, the velocity change seems to be negligible. Silicone oil has a low surface tension $\gamma = 21 \text{ mN/m}$. When a water drop is placed on a silicone oil-infused surface, the oil spreads over

the water surface and covers it.⁵² As a result, a water drop sliding off this designed slippery superhydrophobic surface will also take some oil with it. Therefore, we need more sensitive methods to check this oil depletion. To test how fast oil is removed per drop, we measured the surface tension of the water collected after sliding over a liquid-coated superhydrophobic surface. In addition, we applied proton nuclear magnetic resonance (^1H NMR) to determine the amount of depleted oil in the collected water (Figure 5a).

The control sample for the oil depletion comparison that we use is a slippery smooth liquid-infused PDMS brush surface. This ensures continuous mobility of the oil layer throughout the experimental measurements. In the case of LIS where the depletion of oil volume becomes substantial after multiple drops slide on the surface, the presence of surface roughness introduces complexity in the oil depletion process. To measure the surface tension of water drops sliding over the L-PDMS-SH (7.5%) surface, $45 \mu\text{L}$ water drops were deposited at the top of inclined samples (tilting angle: 50°) by a pump at a speed of $10 \mu\text{L/s}$. The drops slid off the surface and were then collected in a beaker. After different numbers of drops slid over the surfaces, the beaker was placed in a Wilhelmy plate instrument (PT 11 mode of Dataphysics DCAT 25, Wilhelmy plate length: 10 mm;

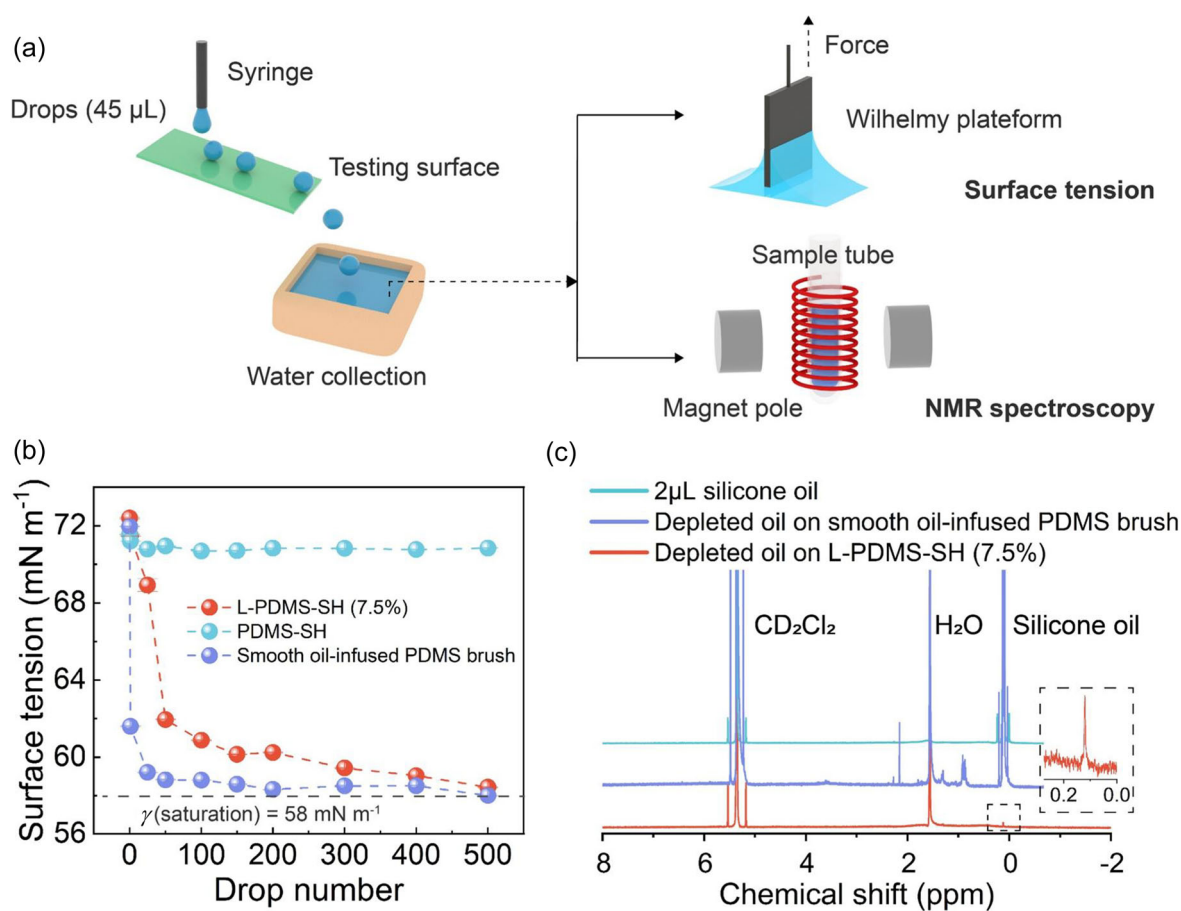


FIGURE 5 Oil depletion. (a) Schematic showing two methods to test the stability of a liquid nanofilm coating on the surface. (b) Interfacial surface tension changes of the collected water after drops slide off different surfaces. (c) Proton nuclear magnetic resonance (NMR) result showing the relative amount of depleted oil after 500 cycles of sliding of drops off the surfaces. L-PDMS-SH, liquid-coated polydimethylsiloxane brush-modified superhydrophobic; PDMS, polydimethylsiloxane; PDMS-SH, PDMS brush-modified superhydrophobic.

width: 19.9 mm; thickness: 0.2 mm) and the surface tension was measured. The oil film will collect on top of the water and decrease the overall surface tension. To measure the interfacial tension of silicone-water plus silicone-air, we added 2 μL of silicon oil in a beaker filled with water. The interfacial tension for the interface in saturation was 58 mN/m (Figure 5b, black dashed line).

When the drop slid off the slippery smooth liquid-infused surface, the surface tension of the collecting water decreased to 62 mN/m even after one drop (Figure 5b). After collecting 50 drops, the surface tension of the water was close to the saturated surface tension. For the L-PDMS-SH (7.5%) surface, the surface tension of the collected water decreased more slowly. After 10 drops slid off the surface, the surface tension only changed from 72 to 69 mN/m. After 500 drops slid off the surface, it reached the saturated surface tension. This result illustrates that the oil depletion volume per sliding drop is lowered on the L-PDMS-SH (7.5%) surface compared to that on a smooth oil-infused surface.

We use ^1H NMR measurement to compare the total amount of depleted oil on these two surfaces. Five hundred water drops slid off the surface and were collected. The collected water was evaporated at 60°C under vacuum for 24 h. The remaining oil was then dissolved in deuterated dichloromethane (CD_2Cl_2) for the ^1H NMR measurement. As a control, we dissolved 2 μL of silicone oil in CD_2Cl_2 . The chemical shift of silicon oil was found to be around 0.1 ppm (^1H NMR) as reported before.⁵⁸ The spectra show that the relative peak integral of depleted oil from L-PDMS-SH (7.5%) (Figure 5c, inset) to that from the smooth tethered liquid surface was 1:22. The collected water drops that slid over the smooth oil-infused PDMS brush surface had a substantially higher amount of oil. During these experiments on the L-PDMS-SH (7.5%) surface, the thickness of oil changed substantially, after 500 drops slid over the surface (Supporting Information: Figure S18). This is because of the replenishing from the bottom oil “reservoir.” This kind of surface shows a longer lifetime when we extend it to include 10,000 drops (Supporting Information: Figure S19). These two results show that the lubricant is depleted more easily from the smooth surfaces than that from L-PDMS-SH (7.5%) surfaces. We suggest that this is because of the reduced contact area and sufficiently thin oil layer,⁵⁹ which is stabilized because it is chemically identical to the brush⁴⁰ and due to the considerable roughness of the surface.⁶⁰

To determine how oil depletion affects the bottom oil “reservoir” at the same time, we studied the electric charging of sliding drops (Supporting Information: Section 5). Water drops spontaneously acquire a charge when they slide on hydrophobic, insulating surfaces.^{61–63} The drop charge on the LIS was found to be affected by the bulk oil layer thickness.⁶⁴ We can determine if oil depletion will affect the thickness of the bottom oil layer on L-PDMS-SH surfaces by varying the charge of sliding drops (Supporting Information: Figure S20a). The increasing drop charge, when the number of drops is low, indicates that the bulk oil layer thickness decreases due to depletion on a slippery L-PDMS-SH (100%). However, this phenomenon cannot be observed when the infusing oil concentration is low, indicating that there is no loss (see Supporting Information: Figure S20b–d).

To test the icing delay time (the time interval between the surface cooling to a certain temperature and ice formation) on the surfaces, we placed 10 μL water drops on a cooling platform THMSG600 (Linkam Scientific Instruments) inside a closed, insulated chamber (Supporting Information: Figure S23). The humidity inside was controlled by mixing certain volumes of dry and wet nitrogen gas. The surface temperature was calibrated versus the temperature in the chamber (Supporting Information: Figure S24). The cooling platform could be cooled down to -20°C and heated up to 20°C at a rate of $0.5^\circ\text{C}/\text{s}$.

Figure 6a shows the freezing and melting process of one water drop on the L-PDMS-SH (7.5%) surface. When the characteristic tip of the spherical ice was observed, the drop was fully frozen.⁶⁵ The surface could remain superhydrophobic after this process. After 10 freezing/melting cycles, we measured the friction force required to move a 10 μL water drop on the surface using a drop adhesion force instrument.^{66,67} The result (Supporting Information: Section 6) shows that compared to that on PDMS-SH surface, the maximum force for a water drop on L-PDMS-SH (7.5%) to start moving did not change a lot after the 10 cycles of test. This means that the mobile oil layer can prevent defect formation due to the drop during the melting process. We have also measured the apparent contact area change of sessile water drops on cooling and heating the surface (Figure 6b). On flat fluorinated glass (F-glass), the contact area remained constant during freezing and melting. On superhydrophobic PDMS-SH and F-SH (fluorinated candle-soot-templated surface), the contact area increased during the freezing process, but it did not decrease after melting. The contact line was pinned. This observation indicates that some defects were generated by an ice/water mixture during the melting. Only for L-PDMS-SH (7.5%) did the contact area increase slightly before the freezing process. After melting, the drop contact area decreased to its original area. The results showed that the mobile contact line^{33,68} of the oil-infused PDMS brush can help to protect superhydrophobicity at low temperatures. Due to this mobility of the contact line, the surface can maintain its performance after more freeze/thaw cycles compared to previously reported work (Supporting Information: Figure S26).

On the L-PDMS-SH (7.5%) surface, freezing was delayed. We measured the delay time on four kinds of surfaces at a surface temperature of -15°C and a humidity of 20%. The tethered liquid nanofilm helps reduce the nucleation sites for the low-temperature water, so that the delay icing time on L-PDMS-SH (7.5%) surfaces was observed to be the longest before freezing (Figure 6c). The long delay in ice formation indicates a low ice nucleation rate.²⁶

In many applications, preventing icing from impacting cooled drops is important. We checked the drop impact process by placing these three surfaces on a Peltier with a surface temperature of -15°C . The high-speed camera, the Peltier, and the syringe were all stored in a refrigerator at 0°C and 20% humidity. A 0°C water drop was released from a syringe at a height of 0.5 cm. The PDMS-SH surface had a low icing delay time and many crystal sites so that the low-velocity cooled water drop did not rebound from the surface (Figure 6d). On the L-PDMS-SH (7.5%) surface, water drops easily

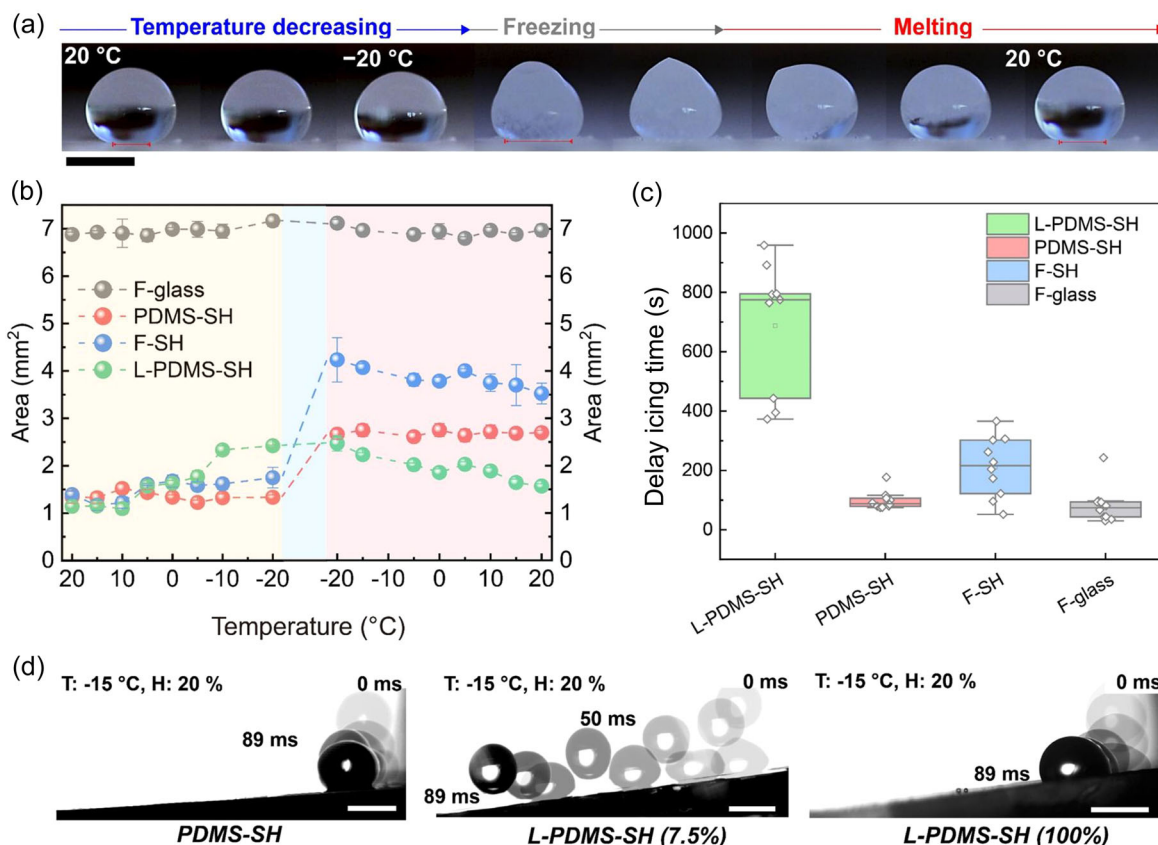


FIGURE 6 Improved icephobicity. (a) Image series showing the freezing and melting process of a 10 μL sessile water drop on the liquid-coated polydimethylsiloxane brush-modified superhydrophobic (L-PDMS-SH) (7.5%) surface. Scale bar: 2 mm. Surface temperature: -15°C ; humidity: 20%. (b) Contact area changes of a sessile water drop on four kinds of surfaces during the freezing and melting process. Yellow part (■): Cooling process. Blue part (■): Freezing process. Red part (■): Melting process. (c) Delay icing time of a sessile 10 μL water drop at -15°C on four different surfaces: L-PDMS-SH (7.5%), PDMS brush-modified superhydrophobic (PDMS-SH), fluorinated superhydrophobic surface (F-SH), and F-glass. (d) Drop impact on L-PDMS-SH (100%), PDMS-SH, and L-PDMS-SH (7.5%) surfaces in 89 ms, $We = 2.15$. Surface titling angle: 5° . Scale bar: 4 mm.

detach from this slightly tilted surface (titling angle: 5°) in a short time. For the surface in a slippery state, water drops will slide for a short distance at the beginning because of the initial energy. Water drops need quite a long time to slide over the surface (200 times longer than that on the superhydrophobic surface)⁶⁹ and it will be frozen on the surface in the end.

CONCLUSION

By coating the brush-modified nanostructure with liquid PDMS, we were able to create nanoscopic liquid-coated surfaces on which water drops form a Cassie state. The liquid nanofilm on top could be replenished from a micrometer-thick bottom oil layer hidden inside the nanostructure. The thickness and distribution of the oil-infused brush were obtained from AFM force measurements. The shedding velocity of liquid-coated surfaces was comparable to those observed on dry superhydrophobic surfaces. This liquid-coated superhydrophobic surface shows enhanced chemical stability based on the liquid nanofilm acting as a sacrificial and replenishable layer. After chemical

etching with an oxygen plasma, the surface recovered to the Cassie state due to the flow and exchange between the two-level oil layers. Oil depletion is quite low on the L-PDMS-SH (7.5%) surface compared to that on a slippery liquid-infused smooth or porous surface. The infused oil reduces the nucleation of cooled water drops and they have the highest icing delay time on the low-temperature liquid-coated superhydrophobic surface. Water drops can easily detach from this cooled surface. This new coating strategy helps us to fabricate robust superhydrophobic surfaces with high chemical stability, maintaining their superliquid repellency at low temperatures. This will be beneficial for the manufacture of long-term, self-cleaning, and corrosion-resistant devices used at low temperatures.

MATERIALS AND METHODS

Surface preparation: Soot-templated surfaces were fabricated as described before⁹: glass slides ($4 \times 2 \text{ cm}^2$; Eprelia) were held 3 cm above the flame of a paraffin candle and moved back and forth for 30 s until they were coated with a black soot layer. The soot-coated

glass substrates were placed in a desiccator together with two open glass vessels containing 4 mL of tetraethoxysilane (TEOS, 98%; Sigma-Aldrich) and aqueous ammonia solution (25%; VWR Chemicals). The desiccator was closed and chemical vapor deposition of TEOS was carried out for 48 h. Then, the surfaces were annealed at 550°C for 2 h in air to remove the carbon cores. After treatment with oxygen plasma (5 min, 200 W, Femto low-pressure plasma system; Diener electronic GmbH) to increase reactivity, the slides were placed in 100 mL of silicon oil (100 cst, 6000 g/mol; Acros Organics) at 150°C for 24 h. Finally, they were immersed in a toluene environment for more than 10 min, and this process was repeated for three times to fully remove unbound PDMS. We call this PDMS layer “brush” here as in previous reports, although it is not clear if the bond to the substrate is really at the end of the chain and if the polymer chain conformation is highly stretched or not.

Silicon oil (100 cst, 6000 g/mol) was dissolved in toluene at concentrations of 100, 80, 60, 40, 20, 15, 10, 7.5, 5, 1, 0.1, 0.01, and 0 wt%. Then, 0.5 mL of these oil solutions was spin-coated (4000 rpm, 60 s) on the PDMS-SH surfaces. To evaporate the solvent, the surfaces were placed on a horizontal plate at 60°C for 1 h.

For comparison, we also prepared fluorinated surfaces. The candle-soot-templated surface was treated with oxygen plasma (5 min, 200 W) to increase reactivity. Then, the surface was placed in a vacuum desiccator containing a dish with 50 μL of 1H,1H,2H,2H-perfluorooctadecyltrichlorosilane (97%; Sigma-Aldrich). The desiccator was evacuated to 80–100 mbar. The reaction was allowed to proceed for 2 h. Finally, the surfaces were rinsed with ethanol to remove unbound silanes.

Silicon oil (100 cst) was dissolved in hexane in a weight ratio of 7.5 wt%. Hexane was used as a solvent because in penetrating the soot layer, toluene solutions were repelled. Then, 0.5 mL of this oil solution was spin-coated (4000 rpm, 60 s) on the fluorinated candle-soot-templated surface. The surface was placed on a horizontal plate at 60°C for 1 h to obtain the LIS.

Smooth lubricated PDMS brush surfaces were prepared as reported before.^{40,41,70} The glass slides were cleaned successively in hexane and alcohol with sonication for 3 min. Then, the glass slides were treated with oxygen plasma (5 min, 200 W). They were immersed in 100 mL of silicone oil (100 cst) at 150°C for 24 h. Then, the surfaces were rinsed with toluene three times. After that, silicon oil (100 cst) was spin-coated on the surfaces in 4000 rpm for 60 s. The oil-infused surfaces were then gently rinsed with ethanol ($\geq 99.8\%$; Honeywell) and Milli-Q water successively to remove nontethered oil.

To characterize the fluorinated surface, we also prepared samples on smooth glass slides. The glass slides were cleaned successively in hexane and alcohol with sonication for 3 min. Then, they were fluorinated as the F-SH surfaces.

Characterization: The morphology of the surface was characterized by SEM (Zeiss LEO 1530 Gemini) at gun voltages of 1.5–3 kV using both the in-lens (for top view) and the SE2 detector (for cross-section view). To avoid charging, samples were sputtered with 7 nm Pt before measurement using a BalTec MED 020 modular high-vacuum coating system (argon pressure of 2×10^{-5} bar, current of 30 mA).

Advancing and receding contact angles as well as the roll-off angles of water on the surface were measured using an OCA 35 goniometer (DataPhysics Instruments). Side view videos of sessile drops were recorded on changing the volume of a sessile water drop gradually (0.5 $\mu\text{L/s}$) between 10 and 20 μL using a Hamilton syringe. Advancing and receding contact angles were determined by fitting an ellipse model to the contour images. Each data point is the average of at least three individual measurements on different areas of the surface.

The oil detection experiment was performed with cantilevers with a nominal resonance frequency of $f = 70$ kHz and a nominal spring constant of $k = 2$ N/m (Brucker OLTESPA). Spring constants were also measured using the thermal tune method. Samples were imaged using the JPK NanoWizard 4 AFM. The so-called QI mode was used to obtain force–distance curves at every point of the 128×128 pixel size scanning area ($3 \times 3 \mu\text{m}^2$ at a set point of 5 nN, a z length of 1 μm , and a time per pixel of 20 ms). To image the presence of oil on the samples, we looked at the instantaneous jump in the cantilever deflection signal on the approach cycle of the force–distance curves due to surface tension forces. The piezo position value at this point of the cantilever jump was subtracted from its position at the end of the approach cycle to obtain the “jump-in distance.” High values of jump-in distance indicate the presence of liquid on the sample surface. The jump-in distance was calculated for each force curve of the scan area automatically using a custom Python script (https://github.com/PranavSudersan/afm_surface_tension/blob/main/AFM_Liquid_Analyzer.ipynb).

^1H NMR measurement was used to determine the volume of depleted oil in the collected water. A 50 mL storage bottle was cleaned with Milli-Q water, ethanol, and acetone successively. After that, the bottle was heated at 60°C under vacuum to remove the residuals. The water drops sliding over the surface were collected in the bottle. The collected water was evaporated at 60°C for more than 24 h to obtain the depleted oil. The oil was then dissolved in CD_2Cl_2 (Deutero GmbH). The ^1H -NMR spectra were recorded on an AVANCE III Bruker NMR spectrometer (500 MHz) at 298 K with 16 scans and a relaxation delay of 12 s. The spectra were calibrated at 5.36 ppm with the remaining proton signal CHDCl_2 signal of the deuterated solvent.

Drop velocity was measured by a tilted platform as reported before⁷¹ by sliding 33 μL drops of distilled water (Thermo Fisher Scientific) over the surfaces. Drops were deposited at the top of a tilted sample by a grounded syringe needle (1.5 mm outer diameter), which was connected to a peristaltic pump (10 $\mu\text{L/s}$, MINIPULS 3; Gilson). The drops fell from a height of ≈ 5 mm, which is similar to the drop size to avoid drop rebounding. Drops were neutralized by a grounded copper wire before they landed on the surface. We imaged the drop with a frame rate of 1000 or 2000 per second on the side over a length of typically 4.5 cm with a high-speed camera (FASTCAM Mini UX100 [Photron] with a TitanTL telecentric lens, $\times 0.268$, 1 in., C-mount [Edmund Optics]). The videos were analyzed by an open drop-shape analysis from MATLAB. The dynamic contact angles were determined by applying a polynomial fit to every frame

of the images. Finally, we determined the drop velocity U by video analysis. All the measurements were performed at a temperature of $20 \pm 1^\circ\text{C}$ and humidity of 20%–40%.

ACKNOWLEDGMENTS

This project received funding from the European Research Council (ERC) under the European Union's Horizon 2020 research and innovation program (Grant agreement nos. 883631, DYNAMO). X. Z. is sponsored by the China Scholarship Council (CSC). We also acknowledge financial support from the German Research Society via the CRC 1194 (Project ID 265191195) project C07N (to C. H.). We are grateful for the technical help in SEM imaging provided by Gunnar Glasser.

CONFLICT OF INTEREST STATEMENT

The authors declare no conflict of interest.

ORCID

Pranav Sudersan  <http://orcid.org/0000-0003-2629-6535>

Hans-Jürgen Butt  <http://orcid.org/0000-0001-5391-2618>

REFERENCES

- Haechler I, Park H, Schnoering G, et al. Exploiting radiative cooling for uninterrupted 24-hour water harvesting from the atmosphere. *Sci Adv*. 2021;7:eabf3978.
- Schutzius TM, Jung S, Maitra T, Graeber G, Köhne M, Poulikakos D. Spontaneous droplet trampolining on rigid superhydrophobic surfaces. *Nature*. 2015;527:82-85.
- Wang D, Sun Q, Hokkanen MJ, et al. Design of robust superhydrophobic surfaces. *Nature*. 2020;582:55-59.
- Zhang W, Shi Z, Zhang F, Liu X, Jin J, Jiang L. Superhydrophobic and superoleophilic PVDF membranes for effective separation of water-in-oil emulsions with high flux. *Adv Mater*. 2013;25:2071-2076.
- Zhang S, Huang J, Chen Z, Lai Y. Bioinspired special wettability surfaces: from fundamental research to water harvesting applications. *Small*. 2017;13:1602992.
- Wang L, Tian Z, Jiang G, et al. Spontaneous dewetting transitions of droplets during icing & melting cycle. *Nat Commun*. 2022;13:378.
- Kreder MJ, Alvarenga J, Kim P, Aizenberg J. Design of anti-icing surfaces: smooth, textured or slippery? *Nat Rev Mater*. 2016;1:15003.
- Tuteja A, Choi W, Ma M, et al. Designing superoleophobic surfaces. *Science*. 2007;318:1618-1622.
- Deng X, Mammen L, Butt H-J, Vollmer D. Candle soot as a template for a transparent robust superamphiphobic coating. *Science*. 2012;335:67-70.
- Artus GRJ, Jung S, Zimmermann J, Gautschi HP, Marquardt K, Seeger S. Silicone nanofilaments and their application as superhydrophobic coatings. *Adv Mater*. 2006;18:2758-2762.
- Li L, Li B, Dong J, Zhang J. Roles of silanes and silicones in forming superhydrophobic and superoleophobic materials. *J Mater Chem A*. 2016;4:13677-13725.
- Ma M, Hill RM. Superhydrophobic surfaces. *Curr Opin Colloid Interface Sci*. 2006;11:193-202.
- Zhang W, Wang D, Sun Z, Song J, Deng X. Robust superhydrophobicity: mechanisms and strategies. *Chem Soc Rev*. 2021;50:4031-4061.
- Jin H, Tian X, Ikkala O, Ras RHA. Preservation of superhydrophobic and superoleophobic properties upon wear damage. *ACS Appl Mater Interfaces*. 2013;5:485-488.
- Chang F-M, Hong S-J, Sheng Y-J, Tsao H-K. High contact angle hysteresis of superhydrophobic surfaces: hydrophobic defects. *Appl Phys Lett*. 2009;95:064102.
- Gennes P-G, Brochard-Wyart F, Quéré D. *Capillarity and Wetting Phenomena: Drops, Bubbles, Pearls, Waves*. Springer; 2004.
- Ducom G, Laubie B, Ohannessian A, Chottier C, Germain P, Chatain V. Hydrolysis of polydimethylsiloxane fluids in controlled aqueous solutions. *Water Sci Technol*. 2013;68:813-820.
- Feng L, Yang Z, Zhai J, et al. Superhydrophobicity of nanostructured carbon films in a wide range of pH values. *Angew Chem Int Ed*. 2003;42:4217-4220.
- Wang C-F, Wang Y-T, Tung P-H, et al. Stable superhydrophobic polybenzoxazine surfaces over a wide pH range. *Langmuir*. 2006;22:8289-8292.
- Peng C, Chen Z, Tiwari MK. All-organic superhydrophobic coatings with mechanochemical robustness and liquid impalement resistance. *Nat Mater*. 2018;17:355-360.
- Chen L, Guo Z, Liu W. Outmatching superhydrophobicity: bio-inspired reentrant curvature for mighty superamphiphobicity in air. *J Mater Chem A*. 2017;5:14480-14507.
- Wu S, Du Y, Alsaïd Y, et al. Superhydrophobic photothermal icephobic surfaces based on candle soot. *Proc Natl Acad Sci USA*. 2020;117:11240-11246.
- Flamm DL, Donnelly VM, Ibbotson DE. Basic chemistry and mechanisms of plasma etching. *J Vac Sci Technol B*. 1983;1:23-30.
- Vali G, DeMott PJ, Möhler O, Whale TF. Technical note: a proposal for ice nucleation terminology. *Atmos Chem Phys*. 2015;15:10263-10270.
- Liu K, Wang C, Ma J, et al. Janus effect of antifreeze proteins on ice nucleation. *Proc Natl Acad Sci USA*. 2016;113:14739-14744.
- Zhang R, Hao P, Zhang X, He F. Supercooled water droplet impact on superhydrophobic surfaces with various roughness and temperature. *Int J Heat Mass Transfer*. 2018;122:395-402.
- Schremb M, Roisman IV, Tropea C. Normal impact of supercooled water drops onto a smooth ice surface: experiments and modelling. *J Fluid Mech*. 2018;835:1087-1107.
- Wang Q, Sun G, Tong Q, Yang W, Hao W. Fluorine-free superhydrophobic coatings from polydimethylsiloxane for sustainable chemical engineering: preparation methods and applications. *Chem Eng J*. 2021;426:130829.
- Wong TS, Kang SH, Tang SKY, et al. Bioinspired self-repairing slippery surfaces with pressure-stable omniphobicity. *Nature*. 2011;477:443-447.
- Lee J, Shin S, Jiang Y, Jeong C, Stone HA, Choi C-H. Oil-impregnated nanoporous oxide layer for corrosion protection with self-healing. *Adv Funct Mater*. 2017;27:1606040.
- Li J, Ueda E, Paulssen D, Levkin PA. Slippery lubricant-infused surfaces: properties and emerging applications. *Adv Funct Mater*. 2019;29:1802317.
- Zhao H, Sun Q, Deng X, Cui J. Earthworm-inspired rough polymer coatings with self-replenishing lubrication for adaptive friction-reduction and antifouling surfaces. *Adv Mater*. 2018;30:1802141.
- Li X, Yang J, Lv K, et al. Salvinia-like slippery surface with stable and mobile water/air contact line. *Natl Sci Rev*. 2021;8:nwaa153.
- Dong Z, Schumann MF, Hokkanen MJ, et al. Superoleophobic slippery lubricant-infused surfaces: combining two extremes in the same surface. *Adv Mater Deerfield*. 2018;30:1803890.
- Launay G, Sadullah MS, McHale G, Ledesma-Aguilar R, Kusumaatmaja H, Wells GG. Self-propelled droplet transport on shaped-liquid surfaces. *Sci Rep*. 2020;10:14987.
- Jenner E, D'Urso B. Wetting states on structured immiscible liquid coated surfaces. *Appl Phys Lett*. 2013;103:251606.
- Villegas M, Zhang Y, Abu Jarad N, Soleymani L, Didar TF. Liquid-Infused surfaces: a review of theory, design, and applications. *ACS Nano*. 2019;13:8517-8536.

38. Teisala H, Geyer F, Haapanen J, et al. Ultrafast processing of hierarchical nanotexture for a transparent superamphiphobic coating with extremely low roll-off angle and high impalement pressure. *Adv Mater.* 2018;30:1706529.
39. Lhermerout R, Davitt K. Contact angle dynamics on pseudo-brushes: effects of polymer chain length and wetting liquid. *Colloids Surf A.* 2019;566:148-155.
40. Chen L, Park S, Yoo J, et al. One-step fabrication of universal slippery lubricated surfaces. *Adv Mater Interfaces.* 2020;7:2000305.
41. Teisala H, Baumli P, Weber SAL, Vollmer D, Butt H-J. Grafting silicone at room temperature—a transparent, scratch-resistant nonstick molecular coating. *Langmuir.* 2020;36:4416-4431.
42. Zhao X, Khatir B, Mirshahidi K, Yu K, Kizhakkedathu JN, Golovin K. Macroscopic evidence of the liquidlike nature of nanoscale polydimethylsiloxane brushes. *ACS Nano.* 2021;15:13559-13567.
43. Leslie DC, Waterhouse A, Berthet JB, et al. A bioinspired omniphobic surface coating on medical devices prevents thrombosis and biofouling. *Nat Biotechnol.* 2014;32:1134-1140.
44. Peppou-Chapman S, Neto C. Depletion of the lubricant from lubricant-infused surfaces due to an air/water interface. *Langmuir.* 2021;37:3025-3037.
45. Huang Y, Stogin BB, Sun N, Wang J, Yang S, Wong T-S. A switchable cross-species liquid repellent surface. *Adv Mater.* 2017;29:1604641.
46. Dai X, Stogin BB, Yang S, Wong T-S. Slippery Wenzel state. *ACS Nano.* 2015;9:9260-9267.
47. Wooh S, Vollmer D. Silicone brushes: omniphobic surfaces with low sliding angles. *Angew Chem Int Ed.* 2016;55:6822-6824.
48. Okumura K, Chevy F, Richard D, Quéré D, Clanet C. Water spring: a model for bouncing drops. *Europhys Lett.* 2003;62:237-243.
49. Deng X, Schellenberger F, Papadopoulos P, Vollmer D, Butt H-J. Liquid drops impacting superamphiphobic coatings. *Langmuir.* 2013;29:7847-7856.
50. Tsai P, Pacheco S, Pirat C, Lefferts L, Lohse D. Drop impact upon micro- and nanostructured superhydrophobic surfaces. *Langmuir.* 2009;25:12293-12298.
51. Han X, Li W, Zhao H, Li J, Tang X, Wang L. Slippery damper of an overlay for arresting and manipulating droplets on nonwetting surfaces. *Nat Commun.* 2021;12:3154.
52. Smith JD, Dhiman R, Anand S, et al. Droplet mobility on lubricant-impregnated surfaces. *Soft Matter.* 2013;9:1772-1780.
53. Keiser A, Keiser L, Clanet C, Quéré D. Drop friction on liquid-infused materials. *Soft Matter.* 2017;13:6981-6987.
54. Olin P, Lindström SB, Pettersson T, Wågberg L. Water drop friction on superhydrophobic surfaces. *Langmuir.* 2013;29:9079-9089.
55. Chen Q, Dai L, Gao M, Huang S, Mau A. Plasma activation of carbon nanotubes for chemical modification. *J Phys Chem B.* 2001;105:618-622.
56. Liu S, Zhou H, Wang H, et al. Argon-plasma reinforced superamphiphobic fabrics. *Small.* 2017;13:1701891.
57. Ortiz-Ortega E, Hosseini S, Martinez-Chapa SO, Madou MJ. Aging of plasma-activated carbon surfaces: challenges and opportunities. *Appl Surf Sci.* 2021;565:150362.
58. Malmström J. Quantification of silicone oil and its degradation products in aqueous pharmaceutical formulations by ¹H-NMR spectroscopy. *J Pharm Sci.* 2019;108:1512-1520.
59. Badr RGM, Hauer L, Vollmer D, Schmid F. Cloaking transition of droplets on lubricated brushes. *J Phys Chem B.* 2022;126:7047-7058.
60. Wong WSY, Hegner KI, Donadei V, Hauer L, Naga A, Vollmer D. Capillary balancing: designing frost-resistant lubricant-infused surfaces. *Nano Lett.* 2020;20:8508-8515.
61. Helseth LE. Influence of salt concentration on charge transfer when a water front moves across a junction between a hydrophobic dielectric and a metal electrode. *Langmuir.* 2020;36:8002-8008.
62. Yatsuzuka K, Mizuno Y, Asano K. Electrification phenomena of pure water droplets dripping and sliding on a polymer surface. *J Electrostat.* 1994;32:157-171.
63. Stetten AZ, Golovko DS, Weber SAL, Butt H-J. Slide electrification: charging of surfaces by moving water drops. *Soft Matter.* 2019;15:8667-8679.
64. Li S, Bista P, Weber SAL, Kappl M, Butt H-J. Spontaneous charging of drops on lubricant-infused surfaces. *Langmuir.* 2022;38:12610-12616.
65. Marín AG, Enríquez OR, Brunet P, Colinet P, Snoeijer JH. Universality of tip singularity formation in freezing water drops. *Phys Rev Lett.* 2014;113:054301.
66. Gao N, Geyer F, Pilat DW, et al. How drops start sliding over solid surfaces. *Nat Phys.* 2018;14:191-196.
67. Hinduja C, Laroche A, Shumaly S, et al. Scanning drop friction force microscopy. *Langmuir.* 2022;38:14635-14643.
68. Tan Y, Yang J, Li Y, et al. Liquid-pressure-guided superhydrophobic surfaces with adaptive adhesion and stability. *Adv Mater.* 2022;34:2202167.
69. Hao C, Li J, Liu Y, et al. Superhydrophobic-like tunable droplet bouncing on slippery liquid interfaces. *Nat Commun.* 2015;6:7986.
70. Krumpfer JW, McCarthy TJ. Rediscovering silicones: “unreactive” silicones react with inorganic surfaces. *Langmuir.* 2011;27:11514-11519.
71. Li X, Bista P, Stetten AZ, et al. Spontaneous charging affects the motion of sliding drops. *Nat Phys.* 2022;18:713-719.

SUPPORTING INFORMATION

Additional supporting information can be found online in the Supporting Information section at the end of this article.

How to cite this article: Zhou X, Sudersan P, Diaz D, et al. Chemically robust superhydrophobic surfaces with a self-replenishing nanoscale liquid coating. *Droplet.* 2024;3:e103. doi:10.1002/dro2.103